Two-Dimensional Hexagonal SnSe Nanosheets as Binder-Free Electrode Material for High-Performance Supercapacitors

Bidhan Pandit, Chandradip D. Jadhav, Padmakar G. Chavan, Hemant S. Tarkas, Jaydeep V. Sali, Ram B. Gupta, and Babasaheb R. Sankapal

***Abstract*—In the class typical layered metal chalcogenide family, tin selenide (SnSe) has been explored resolutely as one of the significant binary IV-VI compounds for a wide range of energy storage applications. Two dimensional hexagonal tin selenide nanosheets have been synthesized using a one-pot colloidal method and tested as active electrode for supercapacitors without using any binder. The as-prepared SnSe electrode exhibits a capacitance of 617.9 F/g at a scan rate of 2 mV/s with a good electrochemical stability due to efficient ion transport between electrolyte to active electrode and charge transport between electrode and current collector. The high energy density of 28.5 Wh/kg along with high cyclic stability is due to the morphology assisted electrochemical activity of the electrode. The results indicate that the assembly of binder-free electrode by the proposed facile synthesis route has a promising application in producing high-performance energy storage devices.**

***Index Terms*—Chalcogenides, electrochemical analysis, energy storage, nanosheets, SnSe.**

I. Introduction

THE electrochemical energy storage devices with high energy and power densities are receiving a lot of interest among researchers because of ever increasing demands in renewable energy, hybrid cars, and portable electronics. For use in the electrochemical supercapacitors (SC), we need suitable electroactive material to meet the required criteria. For example, active materials with high conductivity and hierarchical layered structure can improve ion diffusion and charge transport, which will help increase the energy and power densities with cycling stability. The layered metal chalcogenides (LMCs) have suitable electronic structure, physical and chemical characteristics due to their distinct geometric structures enabled by weak interlayer Van der Waals link, enriched phase structure and easy re-stacking ability [1], [2].

Tin-based binary layered chalcogenides in the form of Sn-X (X = S, Se, Te) have been investigated widely due to their potential applications in next generation optical, electronic, and optoelectronic devices [3]. For example, tin telluride (SnTe) and tin sulfide (SnS) have been used in solar cells [4], [5]. Also, SnSe has attracted much attention as economical, earth-abundant, simple, and stable binary compound which can be used in the sustainable photonic and electronic systems [6].

As typical layered metal chalcogenide, tin selenide (SnSe) has been tested in solar cells, thermoelectric and energy storage applications [7]. SnSe exhibits a distinctive electronic structure due to orthorhombic structure (space group: Pnma) with a direct and indirect allowed transition at 1.2 and 0.9 eV, respectively [8]. This material has been prepared by several researchers, for example, Zainal et al. [9] and Pejova et al. [10] synthesized SnSe by adopting a simple chemical bath deposition (CBD) method. SnSe-Al thin film were fabricated by Suguna et al. on glass substrates using thermal evaporation method at a constant pressure of 2 mPa [11]. SnSe thin films were electrochemically deposited by Bicer et al. [12] and Subramanian et al. [13]. Singh et al. [14] prepared monocrystalline tin selenide film by a hot wall epitaxy technique. Drozd et al. [15] used ALD method to synthesize SnSe structures. Butt et al. [16] also prepared extremely pure and single crystalline SnSe nanospheres through thermal evaporation and subsequent condensation method. Qiao et al. [17] fabricated Sn–Se compound by electrochemical atomic layer epitaxy. Dang et al. [18] prepared SnSe thin films synthesized by solid-state reaction. R. Teghil [19] reported laser induced ablation and epitaxial growth of SnSe.

However, the SnSe nanocrystal synthesis for active electrode material is not very effective due to the presence of $SnSe_2$ impurity. Even though noteworthy advancements have been accomplished in the synthesis of SnSe preparation, current

Manuscript received October 28, 2019; revised March 19, 2020; accepted April 14, 2020. Date of publication April 19, 2020; date of current version July 20, 2020. This work was supported in part by the Visvesvaraya National Institute of Technology (VNIT), Nagpur, in part by the Projects DST/TMD/MES/2k16/09 and SERB/CRG/2020/000103, Government of India, and in part by the Consortium For Scientific Research (CSR) Indore, India, under Project CSR-IC-MSRSR-19/CRS-227/2017-2018/1308. Recommended for publication by Associate Editor K. Ngo. *(Corresponding authors: Babasaheb R. Sankapal.)*

Bidhan Pandit and Babasaheb R. Sankapal are with the Nano Materials and Device Laboratory, Department of Physics, Visvesvaraya National Institute of Technology, Nagpur 440010, Maharashtra, India (e-mail: physics.bidhan@gmail.com; brsankapal@gmail.com).

Chandradip D. Jadhav, Padmakar G. Chavan, Hemant S. Tarkas, and Jaydeep V. Sali are with the Department of Physics School of Physical Sciences, Kavayitri Bahinabai Chaudhari North Maharashtra University, Jalgaon 425001, Maharashtra, India (e-mail: cjadhav71@gmail.com; pgchavan@nmu.ac.in; htarkas1989@gmail.com; jvsali@nmu.ac.in).

Ram B. Gupta is with the Department of Chemical & Life Science Engineering, Virginia Commonwealth University, Richmond, VA 23284-3068 USA (e-mail: rbgupta@vcu.edu).

This paper has supplementary downloadable multimedia material available at https://ieeexplore.ieee.org provided by the authors.

Color versions of one or more of the figures in this article are available online at https://ieeexplore.ieee.org.

Digital Object Identifier 10.1109/TPEL.2020.2989097

approaches depend on expensive and toxic routes hindering its desired applications. The two important phases of binary tin selenide are orthorhombic SnSe and hexagonal $SnSe_2$, respectively [20]. Furthermore, there is a challenge to acquire pure phase of SnSe as Sn (II) is likely to be oxidized to Sn (IV). So, pure crystalline SnSe has not been prepared via simple, low-cost, and environment-friendly precursors in aqueous medium with hierarchy in nanostructure. Hence, advancing a facile strategy for shape organized preparation of nanostructured and hierarchical SnSe is greatly anticipated for mutually fundamental properties and practical approaches as well. Ni et al. [21] synthesized SnSe by adopting microwave-assisted synthesis method for achieving a maximum capacitance of 214.3 F/g. Highlighted on SnSe nanocrystals developed on PET wafer (Au-coated), Wang et al. [22] prepared flexible stacked all solid-state supercapacitor which exhibit a specific capacitance of 1.8 mF/cm^2. Zhang et al. [23] achieved an excellent specific capacitance of 228 F/g for as-synthesized SnSe nanosheet. Recently, Zhong et al. [24] prepared large scale self-assembly of SnSe nanosheets through the hot-injection method and reported 5.56 mF/cm^2 as areal specific capacitance. Although routes were successful, the synthesis is further laborious and requires precise reaction media. Along with phase controlled preparation, shape controlled nanomaterials formation is also significant ascribed to the aspect that electrochemical performances greatly depend on structure and morphology altogether. Recently, hierarchical 2-D nanostructures have been receiving attention due to its high surface area, stability, carrier transport, and performance [25]—[27]. The 2-D materials are ideal for constructing flexible ultrathin-film supercapacitors, offering advantages of flexibility, abundant active surfaces with open ion diffusion channels, which can enable the fast transport and storage of ions [28]—[31].

Herein, we report a facile, solution processed and phase controlled synthesis of hierarchical 2-D SnSe nanosheets with hexagonal morphology. The preparation is based on a one-pot colloidal route consisting tin chloride pentahydrate ($SnCl_4$:$5H_2O$), selenium dioxide (SeO_2), phenanthroline and oleylamine (OAM) with heat treatment and in nitrogen atmosphere. The innovative features in this synthesis technique include: (1) expensive, air-sensitive and toxic precursors have been replaced with air-stable and inexpensive SeO_2; (2) the reaction parameters are precisely controlled to obtain pure phase of SnSe; and (3) the synthesis has been optimized for SnSe hierarchical nanostructure with hexagonal morphology. The obtained SnSe nanostructure is tested for its specific capacitance and stability at high charge-discharge density.

II. Experimental

A. Synthesis of 2-D Hexagonal SnSe Nanosheets

Synthesis of 2-D hexagonal SnSe nanosheets was done by one-pot colloidal method (Fig. 1). In brief, tin chloride pentahydrate ($SnCl_4$:$5H_2O$) 0.1 M, selenium dioxide (SeO_2) 0.1 M, 1–10 phenanthroline (1–10 phen) 0.1 M, and 10 ml of oleylamine (OAM) were added in 3-neck flask. Usually, OAM acts as capping ligand as well as reductant and phenanthroline assists to formulate strong complexes with metal ions altogether help to

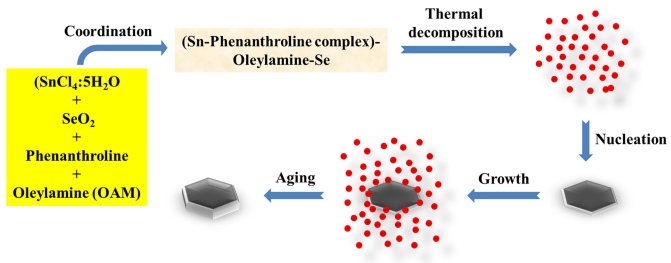

Fig. 1. Schematic of 2-D hexagonal SnSe nanosheets preparation by a one-pot colloidal method.

synthesize SnSe in 2-D hexagonal nanosheet structure [32]. Further, mixture of chemicals in 3-neck flask was stirred vigorously for 5 min and then degassed by ultra high pure (UHP) nitrogen gas. The solution was then heated at 130°C and degassed by UHP N_2 for 10 min. The mixture was again heated at 260°C and aged for 30 min under UHP N_2. The black precipitated product was obtained at bottom of flask. Later on, this product was purified by centrifuging at 4500 r/min for 5 min with addition of ethanol solvent. This centrifugation process was repeated seven times to remove impurities. The obtained purified powder was then used for further characterizations.

The time-dependent growth of the SnSe nanosheets was monitored, which is described in detail in Fig. S1 in the supplementary material. For SnSe nanosheets, in the early reaction stage (30 min ageing), the initially formed SnSe nanocrystals are found to continue to grow with crystalline hexagonal nanosheets, analogous to the PbS nanosheet formation reported by Schliehe et al. [33]. As the shorten reaction time was considered to synthesize thinner nanosheets, there are incomplete hexagonal structures as evident by FESEM image (supplementary Fig. S1a), due to the lack of sufficient time to form hexagonal nanosheets. The nucleation just started in this step; requires more time to grow as full hexagonal sheet in 2-D structure. When the ageing time increases, the newly-formed crystalline SnSe nanosheets could grow out both vertically and laterally, and then assemble into 3-D nanosheets, as shown in supplementary Fig. S1b. Moreover, some agglomeration in a few portions was also seen which is not desired when uniformity is concerned. 2-D nanosheet structure has great advantage to electrochemical performance for electrode material as clearly discussed in previous reports [34], [35] and hence, we restricted the ageing time to 30 minutes as an optimum time for ageing.

B. Electrode Fabrication

Usually, electrodes are prepared by printing or brushing the electrode slurry on the desired substrates. The electrode slurry is normally formed by vigorous stirring of the mixture of binders, conductive agents, and active materials ultrasonically. Various binders have different properties such as polytetrafluoroethylene (PTFE) and polyvinylidene fluoride (PVDF) have great mechanical features but segregate between current collector and active electrode material. On the other hand, carboxymethylcellulose (CMC) maintains good electrochemical characteristics among the polymers but the mechanical feature is very low and cannot be utilized at high temperature (above 40 °C). So, the use

of binders raise concern about the increase in resistivity and decrease in the mechanical strength of the electrodes.

Here, we used a different strategy to fabricate electrode. The nanopowder was dispersed in acetone using sonication for 1 h to get a stable slurry. Afterward, a mirror polished stainless steel (SS) substrate was immersed vertically into the solution for 20 s to adsorb the material onto SS substrate, which was later dried via infrared heating to evaporate the solvent. The complete electrochemical correlation with mass loading has been discussed illustratively in the supplementary material S2. In fact, the mass loading is limited as binder is completely absent in our case. The film surface is well covered without any pinholes and cracks which is beneficial for supercapacitor application. Such surface morphology with nanosized grains offers required channels for electrolyte ions transport in supercapacitor application [36]. In case of higher mass loadings, the films have a tendency to be peeled or scraped off from substrate surface. The cracks in film as specified by supplementary Fig. S3b show the starting of such phase, due to the contact issues with SS substrate.

III. Characterizations

The phase of the prepared SnSe powder was identified by X-ray diffractometer (XRD) using D8 Advance Bruker instrument. Raman studies were performed with LabRAM HR, 532 nm laser excitation. X-ray photoelectron spectroscopy (XPS) analysis was carried out for the samples, using ESCALAB 250 (ThermoElectron) spectrometer with Al Kα excitation source (1486.6 eV). The surface morphology and composition were carried out using field emission scanning electron microscope (FESEM, Model Hitachi S-4800) associated with energy dispersive X-ray spectrometry (EDS). The crystallinity and surface morphology of SnSe powder were further studied by using high resolution transmission electron microscope (HRTEM) and selected area electron diffraction (SAED) (model number, Tecnai G2 20 Twin, FEI).

IV. Result and Discussions

A. Structural Analysis

The XRD pattern of as-synthesized 2-D hexagonal SnSe nanosheets is shown in Fig. 2(a), which clearly indicates that, as-synthesized SnSe is crystalline in nature. All observed diffraction peaks can be index to orthorhombic SnSe phase (JCPDS no. 89-0232, pnma (59)). The absence of any impurity peak indicates the pure phase of SnSe nanosheets [37]—[39]. The detailed crystal structure and lattice parameters are further examined by Rietveld refinement by pseudo-Voigt function (Table I). The refined pattern is denoted by continuous red lines through the observed data points, specified by small black dots. The difference and Bragg diffraction position are shown at the bottom of the pattern in green line and blue ticks, respectively. The calculated profile is in well agreement with experimental pattern, and the refinement results specify orthorhombic structure with lattice parameters of a = 11.385, b = 4.133, and c = 4.446 Å. As shown Fig. 2(b) and (c), the orthorhombic SnSe crystal structure possess layered structure which provides free channels for electrolyte ions to participate intercalation and extraction

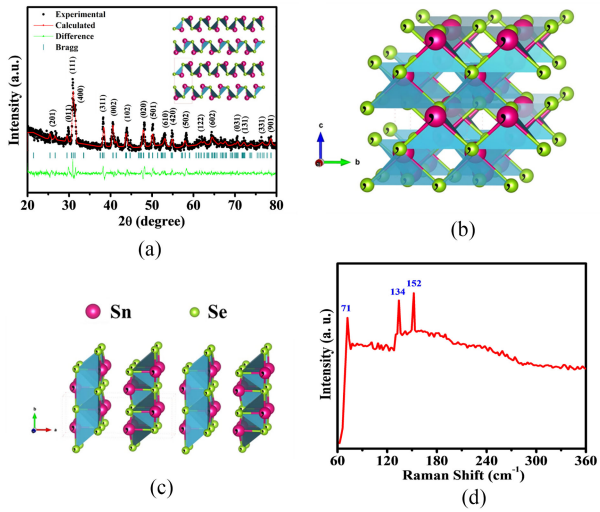

Fig. 2. (a) XRD pattern and Rietveld refinement of SnSe with experimental pattern (black dots), simulated patterns (red line), difference (green line), and Bragg diffraction positions (blue ticks), (b, c) corresponding crystal structures, (d) Raman spectrum of SnSe sample.

TABLE I
Crystallographic Parameters of SnSe Determined by Rietveld Refinement

Formula [molecular weight (g/mol)]	SnSe [197.67]
Crystal system	Orthorhombic
Space group	pnma (#59)
Unit cell parameter (Å)	a = 11.385, b = 4.133, c = 4.446, Z = 4
Unit cell volume (Å^3)	209.236

Atom	x	y	z	Occupancy	$U_{isotropic}$
Sn1	0.0615	0.1250	0.0455	1	1
Se1	0.1785	0.1250	0.0080	1	1

process, clearly favorable to exhibit exceptional electrochemical activity.

As-synthesized SnSe sample was further characterized using Raman analysis. Here, Fig. 2(d) depicts the Raman spectra of hexagonal SnSe nanosheets. Initially, three dominant peaks are found at 71 cm^{-1} is for the A_g mode. The A_g mode corresponds to rigid shear vibration. This observation found in Raman spectra when the incident laser beam is along the a axis [40], [41]. And the other two dominant peaks at 134 and 152 cm^{-1} also gives A_g symmetry [42], [43].

XPS was employed to study the elemental composition and bonding configuration of as-prepared SnSe. As revealed in Fig. 3(a), the high resolution Sn 3d spectrum shows two doublet peaks at 486.4 and 494.8 eV ($3d_{3/2}$), attributed to the Sn (II) [44, 45]. The binding energies for Se $3d_{5/2}$ and $3d_{3/2}$ are 54.1 and 54.9 eV [Fig. 3(b)], confirming the presence of Se (II) [46], [47]. In both the cases, the sharp peaks indicate a single bonding environment with no evidence of a SnO2 peak at 486.7 eV or a Se^{4+} peak in the region of 58–59 eV [48].

B. Morphological Analysis

As-synthesized product of SnSe was further utilized to investigate surface morphology. The typical FESEM images of 2-D hexagonal SnSe nanosheets are shown in Fig. 4(a) and

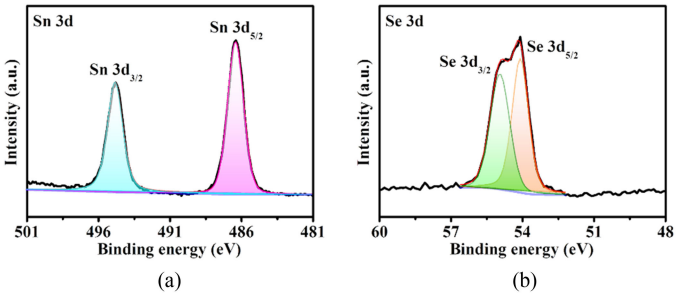

Fig. 3. Core level spectra. (a) Sn 3d. (b) Se 3d.

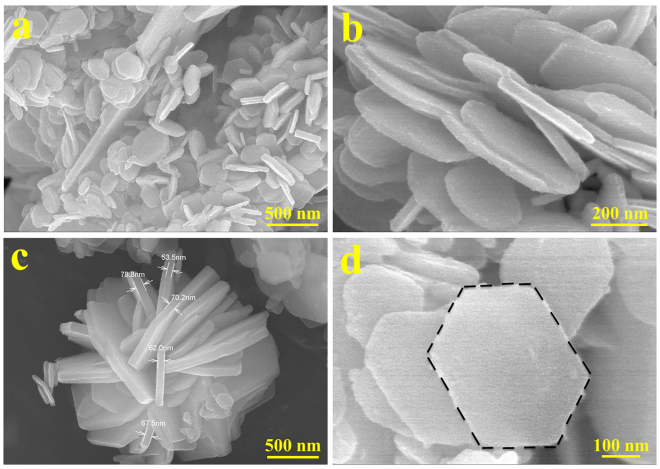

Fig. 4. (a–d) FESEM images of SnSe at different magnifications.

(b) which indicates uniform and large coverage of 2-D hexagonal nanosheets. The average thickness of 2-D hexagonal SnSe nanosheet is found to be 65 nm and is depicted in Fig. 4(c). The formation of hexagonal nanosheet with smooth surface is confirmed from close-up image as shown in Fig. 4(d). EDS elemental mapping was also performed to find the distribution profile of elements for as-synthesized electrode material and results are shown in Fig. 5. The mapping result obviously shows the distribution of Sn and Se elements without existence of any oxide content.

To reveal the crystallinity of 2-D hexagonal SnSe nanosheets, TEM, HR-TEM and SEAD studies have been analyzed and shown in Fig. 6. Fig. 6(a) depicts the bright field image of 2-D hexagonal SnSe nanosheets. Single 2-D hexagonal SnSe nanosheet is shown in Fig. 6(b) which indicates the smooth surface. Fringe spacing 0.3 nm is confirmed from Fig. 6(c) that is consistent with the earlier reports [32], [39]. SAED pattern shown in Fig. 6(d) indicates polycrystalline nature of SnSe nanosheets.

C. Supercapacitor Performance of SnSe Electrodes

The electrochemical behavior of the SnSe electrode were tested using conventional three-electrode configuration with 1 M NaOH aqueous electrolyte. Cyclic voltammetry (CV) is an effective procedure to define the electrochemical properties

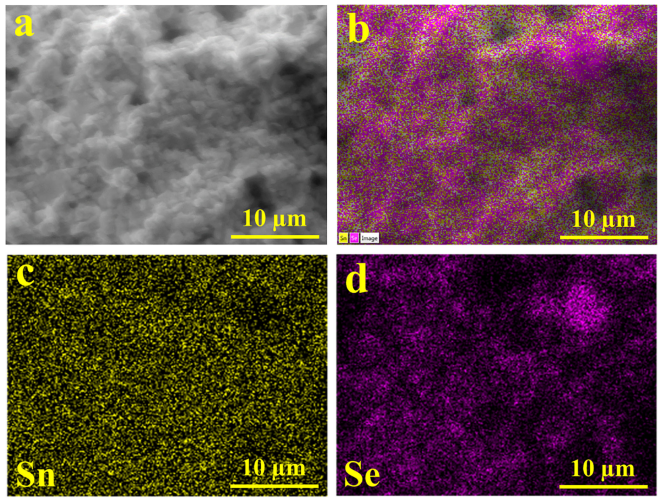

Fig. 5. (a–d) EDS elemental mapping analysis of SnSe electrode.

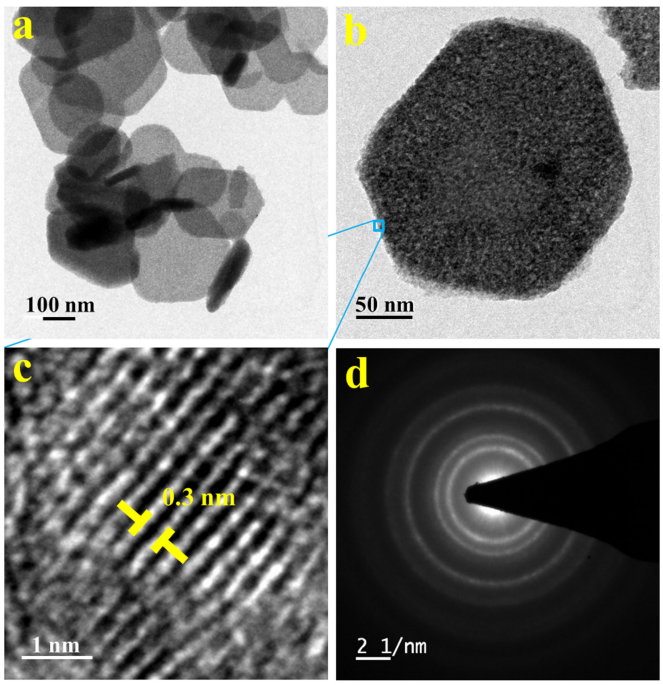

Fig. 6. (a–c) HRTEM images of SnSe. (d) Corresponding SAED pattern.

of synthesized electrode material. CV curves of SnSe electrode shown in Fig. 7(a) are recorded at different scan rates starting from 2 to 100 mV/s, clearly showing a redox couple originating from the reversible reaction of $Sn^{2+} \leftrightarrow Sn^{4+}$ correlating with pseudocapacitive feature of material in the potential range [23]. The CV curve area enlarges in accordance with the rise of scan rate, signifying exceptional capacitive behavior. At upper scan rates, the current response peaks of the electrode increased, suggesting that the material is beneficial to fast redox reactions [49], [50]. The electrochemical parameters of SnSe electrode are estimated using standard equations (supplementary material S4). An extreme capacitance of 617.9 F/g is obtained at the scan rate of 2 mV/s [Fig. 7(b)]. Only the outer surface can involve in

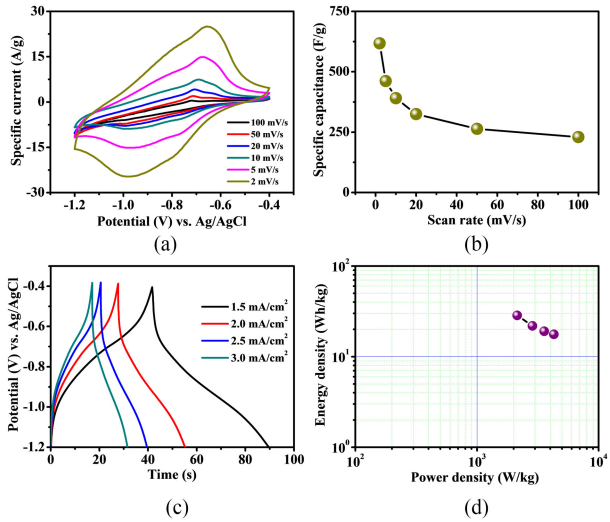

Fig. 7. Electrochemical performance of SnSe electrode in 1 M NaOH electrolyte. (a) CV curves at different scan rates starting from 100 to 2 mV/s. (b) Specific capacitance as a function of scan rate. (c) GCD curves at various current densities starting from 1.5 to 3 mA/cm^2. (d) Ragone plot.

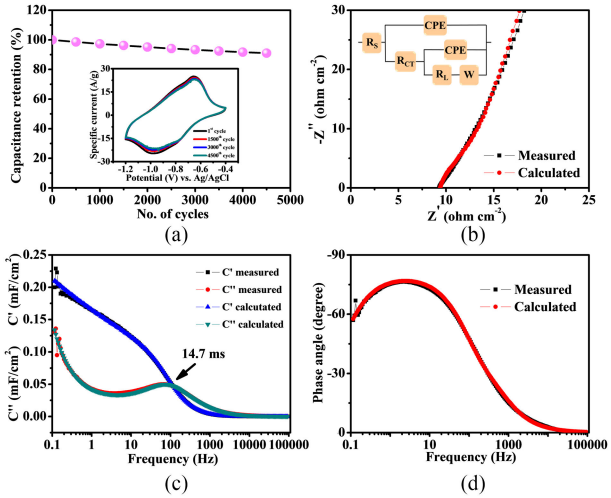

Fig. 8. (a) Cycling steadiness up to 4500 cycles at 100 mV/s scan rate, inset shows CV curves for various cycle numbers. (b) Nyquist plot in frequency range between 100 to 100 kHz. (c) Real and imaginary capacitance against frequency plot. (d) Bode plot.

the capacitive process at faster scan rates with electrolyte ions and results less use of electroactive material compared [51].

The galvanostatic charge-discharge (GCD) curves of the electrode were measured at current densities ranging from 1.5 to 3 mA/cm^2, as depicted in Fig. 7(c). The GCD curves demonstrate well sloping potential plateaus which are consistent with CV curves, approving the pseudocapacitive character of the material whatsoever. The specific capacitance values are calculated from discharge slopes regarding CD plots examined in potential limited regions with different current densities. The plateau with iR drop followed by a sloping curve completely agrees with CV results. The iR drop appeared at the beginning of each discharge curve corresponds to the characteristic internal resistance [52]. The electrode delivers a highest specific capacitance of 320.8 F/g at a definite current density of 1.5 mA/cm^2. The typical phenomenon of supercapacitor is that the capacitance generally drops at relatively greater current density as discharge is much quicker at higher current density compared to lower current densities [53], [54]. Precisely, the active interaction among SnSe and selected electrolyte ions reduces with the rise of current density due to insufficient time constraints, analogous to lack insertion/exertion reaction henceforth poorer capacitance [55].

Ragone energy plot linking the power density to energy density is an effective approach to estimate electrochemical function of electroactive material. Reasonably, the energy density of SnSe electrode can range up to 28.5 Wh/kg at excellent power density of 2.1 kW/kg, also remains 17.6 Wh/kg at power density of 4.3 kW/kg, revealing a wide power range which can be acquired despite of retaining a comparatively great energy density. The outcomes [Fig. 7(d)] clearly demonstrate that SnSe nanosheets provide exceptional electrochemical performance in terms of output energy and power density altogether.

The cyclic steadiness of the electrode was also scanned by reparative CV test for a large number of cycles (4500) at stable scan rate of 100 mV/s. As displayed in Fig. 8(a), 91% of the primary capacitance can be retained even after 4500 cycles, showing a good electrochemical stability. The excellent electrochemical stability can be attributed to the unique hierarchical structure which facilitates first-rate electron transfer and extract/inset electrolyte ions throughout the complete electrochemical cycling process [56].

Fig. 8(b) shows the Nyquist plots of highly sensitive and non-intrusive EIS spectra for the electrode material in 0.1 Hz to 100 kHz frequency range. The spectrum is equivalent with quasi-semicircular segment at high frequency region with linear section at low frequency range. At higher frequencies, the intersection point on real axis signifies the complete internal resistance (Rs), originating from interfacial resistance among current-collector and electrode, ohmic resistance of used electrolyte and inherent electronic resistance electrode material after all [57], [58]. From the Nyquist plot, it can be established that the R_S value is 9.28 Ω, for the electrode. As shown in Fig. 8(b), the diameter of semicircular arc of SnSe electrode is considerably lower (2.6 Ω), signifying as charge transfer resistance (R_{CT}), resulting from quicker transference of charges and ions at electrode-electrolyte interface [59].

These small values are of excessive significance because they not only influence energy and power performance, but diminish unnecessary heat dissipation during GCD cycles via advanced exploitation of active electrode material also [60]. Furthermore, the closely fitted equivalent circuit of Nyquist plot is displayed in the inset of Fig. 8(b). The double layer capacitance appearing at electrode-electrolyte interface is represented by significant constant phase element (CPE) [61]. At relatively lower frequencies, the −45° slope of the Nyquist plot is signified by Warburg element (W), and is directly reliant on frequency while R_L denotes the resistance related to leakage throughout the electrochemical interactions [62]. Fig. 8(c) demonstrates the imaginary (C'') and real (C') parts of capacitance in contrast to frequency limit. The deviation of C'' against frequency displays a maxima at a specified characteristic frequency f_0 (67.9 Hz), outlining relaxation time constant as $\tau_0 = \frac{1}{f_0}$ [63, 64]. Relaxation time

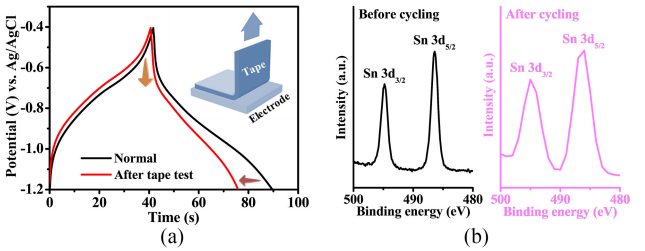

Fig. 9. (a) Charge-discharge curves of SnSe electrode at current density of 1.5 mA/cm^2 before and after tape test. (b) Core level spectra of Sn 3d before and after cycling.

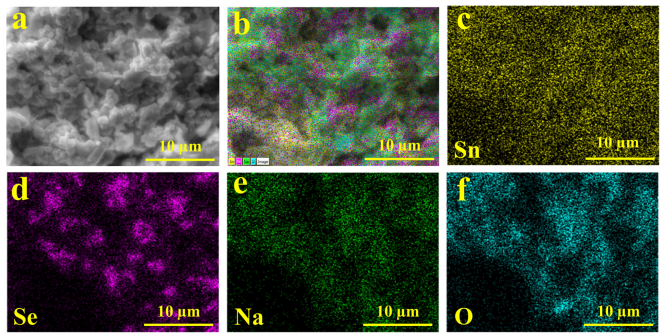

Fig. 10. (a−f) EDS elemental mapping analysis of SnSe electrode after cycling test.

constant is a degree of rate capability of the electrode due to the association with rapid supercapacitive discharge [65]. The τ_0 value is smallest time essential to provide stored energy through an efficiency larger than 50% of its ultimate value and relays the shift between capacitive and resistive actions of supercapacitor [66]. The estimated relaxation time constant of 14.7 ms intends remarkable GCD rate of electroactive material. The imaginary capacitance (C′′) has been easily estimated from experimental impedance data by considering [67], [68]

$$\mathrm{C}'' = \frac{\mathrm{Z}'}{2\pi \mathrm{f} \mid \mathrm{Z}\mid^2}. \tag{1}$$

The analyzed phase angle (−76.4°) is near to −90° as revealed by characteristic Bode plot [Fig. 8(d)], strongly signifying about exceptional capacitive behavior [69]. As resistive and capacitive impedances are indistinguishable at a particular −45° phase angle, so relaxation time constant can also be projected by $\tau_0 = \frac{1}{\mathrm{f}_0}$ at the equivalent phase [70]. The corresponding relaxation time constant is found to be 8.8 ms, relating with the outcomes accomplished from the preceding analysis.

In terms of mechanical characterization, the adherence of the films to the substrates was good and the films were not peeled or scraped off from the SS substrate. For adhesion testing the film was placed in ultrasonic bath for overnight which resulted in negligible change (0.001% of its original) in mass loading of the material.

Adhesion tape is a useful test for evaluating adhesion intensity of materials to the substrate [2]. In this process, the tape has been applied to the electrode surface for number of times and pulled-off rapidly. Then, the electrode was inspected with GCD test at current density of 1.5 mA/cm^2. Though there was slight reduction in discharge time with a minute change in discharge plateau shape after using tape for 10 times, as shown by Fig. 9(a). Moreover, the iR drop increases slightly due to the inclusion of resistive factors with the repetitive tape test.

XPS was employed to study the oxidation state of Sn element in as-prepared SnSe electrode before and after electrochemical cycling studies (4500 cycles). As shown in Fig. 9(b), the high resolution Sn 3d spectrum shows two doublet peaks at 486.4 eV ($3d_{5/2}$) and 494.8 eV ($3d_{3/2}$), attributed to the Sn (II) [44, 45]. The XPS Sn 3-D spectra suggest that that the peak position remained almost unchanged after 4500 CV cycles; a great chemical stability of the material is thus confirmed. In both the cases, the sharp peaks indicate a single bonding environment with no evidence of other Sn-oxidized peaks [48]. Previously reported literature also supports similar XPS analysis associated with post-cycling state of electrode material [71], [72].

The presence of Na and O elements on the surface of SnSe electrode after cyclic stability test as shown by Fig. 10 due to the use of NaOH electrolyte. The SEM image (supplementary Fig. S5) after cycling studies (4500 cycles) shows the non-alteration of hexagonal shape even after stability studies. No obvious difference in the morphology and elemental distribution was found from EDS mapping comparison of the initial state.

V. Conclusion

In summary, we develop a unique hexagonal structured SnSe electrode that shows high capacitance and cycle stability in spite of involved redox mechanism. Employing simple electrode fabrication following the one-pot synthesis route is advantageous towards the industrial use. The electrode shows a high specific capacitance of 617.9 F/g at a scan rate of 2 mV/s with fast charge–discharge cycles. The low charge transfer resistance supports the fast facilitation of electrolyte ions into the electro-active material, showing a power density of 4.3 kW/kg. Due to the rich redox chemistry and high electrochemical activity, SnSe has potential for use in the high-performance SCs combining both high energy and power densities.

References

[1] Y. He *et al.*, "Strain-induced electronic structure changes in stacked van der Waals heterostructures," *Nano Lett.*, vol. 16, pp. 3314–3320, 2016.
[2] Z. Guo, F. Sun, and W. Yuan, "Chemical Intercalations in Layered Transition Metal Chalcogenides: Syntheses, Structures, and Related Properties," *Cryst. Growth Des.*, vol. 17, pp. 2238–2253, 2017.
[3] W. Shi *et al.*, "Tin selenide (SnSe): Growth, properties, and applications," *Adv. Sci.*, vol. 5, 2018, Art. no. 1700602.
[4] Y. Jang *et al.*, "Cation exchange combined with Kirkendall effect in the preparation of SnTe/CdTe and CdTe/SnTe core/shell nanocrystals," *J. Phys. Chem. Lett.*, vol. 7, pp. 2602–2609, 2016.
[5] B.-I. Park, Y. H. Jang, S. Y. Lee, and D.-K. Lee, "Mechanochemically synthesized SnS nanocrystals: Impact of nonstoichiometry on phase purity and solar cell performance," *ACS Sustain. Chem. Eng.*, vol. 6, pp. 3002–3009, 2018.
[6] M. A. Franzman, C. W. Schlenker, M. E. Thompson, and R. L. Brutchey, "Solution-phase synthesis of SnSe nanocrystals for use in solar cells," *J. Am. Chem. Soc.*, vol. 132, pp. 4060–4061, 2010.
[7] S. Yuan *et al.*, "Surfactant-free aqueous synthesis of pure single-crystalline SnSe nanosheet clusters as anode for high energy- and power-density sodium-ion batteries," *Adv. Materials*, vol. 29, 2017, Art. no. 1602469.

[8] P. A. Fernandes, M. G. Sousa, P. M. P. Salomé, J. P. Leitão, and A. F. da Cunha, "Thermodynamic pathway for the formation of SnSe and $SnSe_2$ polycrystalline thin films by selenization of metal precursors," *CrystEngComm*, vol. 15, pp. 10278–10286, 2013.

[9] Z. Zainal, N. Saravanan, K. Anuar, M. Z. Hussein, and W. M. M. Yunus, "Chemical bath deposition of tin selenide thin films," *Materials Sci. Eng.: B*, vol. 107, pp. 181–185, 2004.

[10] B. Pejova and I. Grozdanov, "Chemical synthesis, structural and optical properties of quantum sized semiconducting tin(II) selenide in thin film form," *Thin Solid Films*, vol. 515, pp. 5203–5211, 2007.

[11] P. Suguna, D. Mangalaraj, S. K. Narayandass, and P. Meena, "Structure, composition, dielectric, and AC conduction studies on tin selenide films," *phys. status solidi (a)*, vol. 155, pp. 405–416, 1996.

[12] M. Biçer and İ. Şişman, "Electrodeposition and growth mechanism of SnSe thin films," *Appl. Surface Sci.*, vol. 257, pp. 2944–2949, 2011.

[13] B. Subramanian, T. Mahalingam, C. Sanjeeviraja, M. Jayachandran, and M. J. Chockalingam, "Electrodeposition of Sn, Se, SnSe and the material properties of SnSe films," *Thin Solid Films*, vol. 357, pp. 119–124, 1999.

[14] J. P. Singh and R. K. Bedi, "Thermally stimulated currents in epitaxially grown tin selenide films," *Jpn. J. Appl. Phys.*, vol. 29, pp. L869–L871, 1990.

[15] V. E. Drozd, I. O. Nikiforova, V. B. Bogevolnov, A. M. Yafyasov, E. O. Filatova, and D. Papazoglou, "ALD synthesis of SnSe layers and nanostructures," *J. Phys. D: Appl. Phys.*, vol. 42, 2009, Art. no. 125306.

[16] F. K. Butt *et al.*, "Synthesis of highly pure single crystalline SnSe nanostructures by thermal evaporation and condensation route," *Materials Chem. Phys.*, vol. 137, pp. 565–570, 2012.

[17] Z. Qiao, W. Shang, and C. Wang, "Fabrication of Sn–Se compounds on a gold electrode by electrochemical atomic layer epitaxy," *J. Electroanalytical Chem.*, vol. 576, pp. 171–175, 2005.

[18] T. Q. Dang, "SnSe thin films synthesized by solid state reactions," *Thin Solid Films*, vol. 149, pp. 197–203, 1987.

[19] R. Teghil, A. Giardini-Guidoni, A. Mele, S. Piccirillo, G. Pizzella, and V. Marotta, "Laser induced ablation and epitaxial growth of SnSe," *Thin Solid Films*, vol. 241, pp. 126–128, 1994.

[20] P. Ramasamy, P. Manivasakan, and J. Kim, "Phase controlled synthesis of SnSe and $SnSe_2$ hierarchical nanostructures made of single crystalline ultrathin nanosheets," *CrystEngComm*, vol. 17, pp. 807–813, 2015.

[21] D. Ni, Y. Chen, X. Yang, C. Liu, and K. Cai, "Microwave-assisted synthesis method for rapid synthesis of tin selenide electrode material for supercapacitors," *J. Alloys Compounds*, vol. 737, pp. 623–629, 2018.

[22] X. Wang *et al.*, "Spray-painted binder-free SnSe electrodes for high-performance energy-storage devices," *ChemSusChem*, vol. 7, pp. 308–313, 2014.

[23] C. Zhang *et al.*, "Two-dimensional tin selenide nanostructures for flexible all-solid-state supercapacitors," *ACS Nano*, vol. 8, pp. 3761–3770, 2014.

[24] Y. Zhong *et al.*, "Large scale self-assembly of SnSe nanosheets prepared by the hot-injection method for photodetector and capacitor applications," *Materials Today Energy*, vol. 12, pp. 418–425, 2019.

[25] J. Liao, W. Ni, C. Wang, and J. Ma, "Layer-structured niobium oxides and their analogues for advanced hybrid capacitors," *Chem. Eng. J.*, Art. no 123489, 2019; doi: 10.1016/j.cej.2019.123489.

[26] B. Xu *et al.*, "2020 roadmap on two-dimensional materials for energy storage and conversion," *Chin. Chem. Lett.*, vol. 30, pp. 2053–2064, 2019.

[27] M. Wu *et al.*, "Perspectives in emerging bismuth electrochemistry," *Chem. Eng. J.*, vol. 381, 2020, Art. no. 122558.

[28] C. Wu *et al.*, "Two-dimensional vanadyl phosphate ultrathin nanosheets for high energy density and flexible pseudocapacitors," *Nat. Commun.*, vol. 4, 2013, Art. no. 2431.

[29] L. Peng, X. Peng, B. Liu, C. Wu, Y. Xie, and G. Yu, "Ultrathin two-dimensional MnO2/graphene hybrid nanostructures for high-performance, flexible planar supercapacitors," *Nano Lett.*, vol. 13, pp. 2151–2157, 2013.

[30] Y. Zhu, L. Peng, Z. Fang, C. Yan, X. Zhang, and G. Yu, "Structural engineering of 2D nanomaterials for energy storage and catalysis," *Adv. Materials*, vol. 30, 2018, Art. no. 1706347.

[31] L. Peng, Z. Fang, Y. Zhu, C. Yan, and G. Yu, "Holey 2D nanomaterials for electrochemical energy storage," *Adv. Energy Materials*, vol. 8, 2018, Art. no. 1702179.

[32] L. Li *et al.*, "Single-layer single-crystalline SnSe nanosheets," *J. Amer. Chem. Soc.*, vol. 135, pp. 1213–1216, 2013.

[33] C. Schliehe *et al.*, "Ultrathin PbS sheets by two-dimensional oriented attachment," *Science*, vol. 329, pp. 550–553, 2010.

[34] R. Lv *et al.*, "Transition metal dichalcogenides and beyond: Synthesis, properties, and applications of single- and few-layer nanosheets," *Accounts Chem. Res.*, vol. 48, pp. 56–64, 2015.

[35] Y.-P. Gao, X. Wu, K.-J. Huang, L.-L. Xing, Y.-Y. Zhang, and L. Liu, "Two-dimensional transition metal diseleniums for energy storage application: A review of recent developments," *CrystEngComm*, vol. 19, pp. 404–418, 2017.

[36] V. R. Shinde, S. B. Mahadik, T. P. Gujar, and C. D. Lokhande, "Supercapacitive cobalt oxide (Co_3O_4) thin films by spray pyrolysis," *Appl. Surface Sci.*, vol. 252, pp. 7487–7492, 2006.

[37] D. D. Vaughn, S.-I. In, and R. E. Schaak, "A Precursor-Limited Nanoparticle Coalescence Pathway for Tuning the Thickness of Laterally-Uniform Colloidal Nanosheets: The Case of SnSe," *ACS Nano*, vol. 5, pp. 8852–8860, 2011.

[38] J. Liu *et al.*, "Screw dislocation-driven growth of the layered spiral-type SnSe nanoplates," *Crystal Growth Des.*, vol. 16, pp. 2052–2056, 2016.

[39] J. Liu *et al.*, "High white light photosensitivity of SnSe nanoplate-graphene nanocomposites," *Nanoscale Res. Lett.*, vol. 12, 2017, Art. no. 259.

[40] H. R. Chandrasekhar, R. G. Humphreys, U. Zwick, and M. Cardona, "Infrared and Raman spectra of the IV-VI compounds SnS and SnSe," *Phys. Rev. B*, vol. 15, pp. 2177–2183, 1977.

[41] J. Liu *et al.*, "Large scale SnSe pyramid structure grown by gradient vapor deposition method," *CrystEngComm*, vol. 20, pp. 1037–1041, 2018.

[42] V. R. Minnam Reddy *et al.*, "α-SnSe thin film solar cells produced by selenization of magnetron sputtered tin precursors," *Sol. Energy Materials Sol. Cells*, vol. 176, pp. 251–258, 2018.

[43] V. Kumar, P. Kumar, S. Yadav, V. Kumar, M. K. Bansal, and D. K. Dwivedi, "Growth and characterization of tin selenide films synthesized by low cost technique for photovoltaic device applications," *J. Materials Sci.: Materials. Elecronics*, vol. 27, pp. 4043–4049, 2016.

[44] L. Ling, Q. Zhang, L. Zhu, C.-F. Wang, and S. Chen, "Interfacial synthesis of SnSe quantum dots for sensitized solar cells," *RSC Advances*, vol. 5, pp. 2155–2158, 2015.

[45] L. Das, A. Guleria, S. Neogy, and S. Adhikari, "Porous nanostructures of SnSe: role of ionic liquid, tuning of nanomorphology and mechanistic studies," *RSC Advances*, vol. 6, pp. 92934–92942, 2016.

[46] J. Li *et al.*, "High yield electrochemical exfoliation synthesis of tin selenide quantum dots for high-performance lithium-ion batteries," *J. Materials Chem. A*, vol. 7, pp. 23958–23963, 2019.

[47] X. Yang *et al.*, "Assembly of SnSe nanoparticles confined in graphene for enhanced sodium-ion storage performance," *Chem. Eur. J.*, vol. 22, pp. 1445–1451, 2016.

[48] M. R. Burton *et al.*, "Thin film tin selenide (SnSe) thermoelectric generators exhibiting ultralow thermal conductivity," *Adv. Materials*, vol. 30, 2018, Art. no. 1801357.

[49] B. Pandit, L. K. Bommineedi, and B. R. Sankapal, "Electrochemical engineering approach of high performance solid-state flexible supercapacitor device based on chemically synthesized VS_2 nanoregime structure," *J. Energy Chem.*, vol. 31, pp. 79–88, 2019.

[50] Z. Gao *et al.*, "Catalytic electrode-redox electrolyte supercapacitor system with enhanced capacitive performance," *Chem. Eng. J.*, vol. 335, pp. 590–599, 2018.

[51] S. A. Pande, B. Pandit, and B. R. Sankapal, "Facile chemical route for multiwalled carbon nanotube/mercury sulfide nanocomposite: High performance supercapacitive electrode," *J. Colloid Interface Sci.*, vol. 514, pp. 740–749, 2018.

[52] B. Pandit, V. S. Devika, and B. R. Sankapal, "Electroless-deposited Ag nanoparticles for highly stable energy-efficient electrochemical supercapacitor," *J. Alloys Compounds*, vol. 726, pp. 1295–1303, 2017.

[53] T. Yang, Q. Lu, and S. Zhao, "Monodispersed silica@nickel silicate hydroxide core–shell spheres for supercapacitor electrodes," *phys. status solidi (a)*, vol. 216, 2019, Art. no. 1900395.

[54] S. A. Pande, B. Pandit, and B. R. Sankapal, "Vanadium oxide anchored MWCNTs nanostructure for superior symmetric electrochemical supercapacitors," *Materials Des.*, vol. 182, 2019, Art. no. 107972.

[55] R. Thangappan *et al.*, "Graphene decorated with MoS_2 nanosheets: a synergetic energy storage composite electrode for supercapacitor applications," *Dalton Trans.*, vol. 45, pp. 2637–2646, 2016.

[56] B. Pandit, S. R. Dhakate, B. P. Singh, and B. R. Sankapal, "Free-standing flexible MWCNTs bucky paper: Extremely stable and energy efficient supercapacitive electrode," *Electrochim. Acta*, vol. 249, pp. 395–403, 2017.

[57] B. Pandit, B. R. Sankapal, and P. M. Koinkar, "Novel chemical route for CeO_2/MWCNTs composite towards highly bendable solid-state supercapacitor device," *Sci. Rep.*, vol. 9, 2019, Art. no. 5892.

[58] C.-C. Shih *et al.*, "A rapid and green method for the fabrication of conductive hydrogels and their applications in stretchable supercapacitors," *J. Power Sources*, vol. 426, pp. 205–215, 2019.

[59] B. Pandit, G. K. Sharma, and B. R. Sankapal, "Chemically deposited Bi_2S_3:PbS solid solution thin film as supercapacitive electrode," *J. Colloid Interface Sci.*, vol. 505, pp. 1011–1017, 2017.
[60] W. Si, C. Yan, Y. Chen, S. Oswald, L. Han, and O. G. Schmidt, "On chip, all solid-state and flexible micro-supercapacitors with high performance based on MnO_x/Au multilayers," *Energy Environ. Sci.*, vol. 6, pp. 3218–3223, 2013.
[61] W. Wang *et al.*, "Hydrous ruthenium oxide nanoparticles anchored to graphene and carbon nanotube hybrid foam for supercapacitors," *Sci. Rep.*, vol. 4, 2014, Art. no. 4452.
[62] D. K. Kampouris, X. Ji, E. P. Randviir, and C. E. Banks, "A new approach for the improved interpretation of capacitance measurements for materials utilised in energy storage," *RSC Advances*., vol. 5, pp. 12782–12791, 2015.
[63] B. Pandit, N. Kumar, P. M. Koinkar, and B. R. Sankapal, "Solution processed nanostructured cerium oxide electrode: Electrochemical engineering towards solid-state symmetric supercapacitor device," *J. Electroanalytical Chem.*, vol. 839, pp. 96–107, 2019.
[64] P. Giannakou, M. G. Masteghin, R. C. T. Slade, S. J. Hinder, and M. Shkunov, "Energy storage on demand: ultra-high-rate and high-energy-density inkjet-printed NiO micro-supercapacitors," *J. Materials Chem. A*, vol. 7, pp. 21496–21506, 2019.
[65] B. Pandit and B. R. Sankapal, "Highly conductive energy efficient electroless anchored silver nanoparticles on MWCNTs as a supercapacitive electrode," *New J. Chem.*, vol. 41, pp. 10808–10814, 2017.
[66] P. Xu *et al.*, "Laminated ultrathin chemical vapor deposition graphene films based stretchable and transparent high-rate supercapacitor," *ACS Nano*, vol. 8, pp. 9437–9445, 2014.
[67] B. Pandit, S. A. Pande, and B. R. Sankapal, "Facile SILAR processed Bi2S3:PbS solid solution on MWCNTs for high-performance electrochemical supercapacitor," *Chin. J. Chem.* vol. 37, pp. 1279–1286, 2019.
[68] J. Guo, D. Wu, T. Wang, and Y. Ma, "P-doped hierarchical porous carbon aerogels derived from phenolic resins for high performance supercapacitor," *Appl. Surface Sci.*, vol. 475, pp. 56–66, 2019.
[69] S. A. Pande, B. Pandit, and B. R. Sankapal, "Electrochemical approach of chemically synthesized HgS nanoparticles as supercapacitor electrode," *Materials Lett.*, vol. 209, pp. 97–101, 2017.
[70] S. He and W. Chen, "Application of biomass-derived flexible carbon cloth coated with MnO_2 nanosheets in supercapacitors," *J. Power Sources*, vol. 294, pp. 150–158, 2015.
[71] W. Yuan, L. Cheng, H. Wu, Y. Zhang, S. Lv, and X. Guo, "One-step synthesis of 2D-layered carbon wrapped transition metal nitrides from transition metal carbides (MXenes) for supercapacitors with ultrahigh cycling stability," *Chem. Commun.*, vol. 54, pp. 2755–2758, 2018.
[72] J.-K. Chang, C.-H. Huang, M.-T. Lee, W.-T. Tsai, M.-J. Deng, and I. W. Sun, "Physicochemical factors that affect the pseudocapacitance and cyclic stability of Mn oxide electrodes," *Electrochim. Acta*, vol. 54, pp. 3278–3284, 2009.

Bidhan Pandit received the Ph.D. degree in physics from Visvesvaraya National Institute of Technology, India, in 2019.

Currently, he is working as CNRS Postdoctoral Research Fellow at the Institut Charles Gerhardt Montpellier (ICGM), Université de Montpellier, France. His current scientific interests include synthesis of nanostructures for next-generation energy storage applications (supercapacitors and lithium/sodium ion batteries) and fabrication of flexible energy storage devices to investigate electrochemical behaviors.

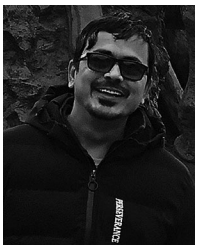

Chandradip D. Jadhav received the master's degree in physics (with specialization in energy studies) from Kavayitri Bahinabai Chaudhari North Maharashtra University, Jalgaon, India, and is currently working toward the Ph.D. degree in material science and engineering with the Wuhan University of Science and Technology, Wuhan, China.

His research interest includes nanomaterial synthesis, field emission, supercapacitor, fuel cell, and Zn-air battery.

Padmakar G. Chavan received the M.Sc. (Phys.) degree with specialization in material science from the Department of Physics, School of Physical Sciences, Kavayitri Bahinabai Chaudhari North Maharashtra University Jalgaon, Jalgaon, India, in 2006, and the Ph.D. degree in field electron emission from the Department of Physics, Savitribai Phule Pune University, Pune, India, in 2012.

He has been an Assistant Professor in physics with the Department of Physics, School of Physical Sciences, Kavayitri Bahinabai Chaudhari North Maharashtra University Jalgaon since 2012. His research interests include ultrahigh vacuum, synthesis of nanomaterials, characterization, field electron emission, etc.

Hemant S. Tarkas was recently awarded with Ph.D. in Physics from KBC North Maharashtra University, Jalgaon (MH), India, in 2019.

Dr. Hemant S. Tarkas was an INSPIRE Fellow-SRF under INSPIRE program DST, New Delhi. His research interest includes the synthesis of nanostructures for various applications including Perovskite solar cell, Organic Inorganic Hybrid solar cells, DSCC, LEDs, Supercapacitor, and Fuel cell materials.

Jaydeep V. Sali received the M.Sc. and Ph.D. degrees in physics from the University of Pune, Pune, India, in 1993 and 2000, respectively.

He is currently a Professor of Physics with the School of Physical Sciences, Kavayitri Bahinabai Chaudhari North Maharashtra University Jalgaon, Jalgaon, India. His research interests include modeling and simulation of thin films growth mechanisms with applications specifically in the field of optoelectronics devices.

Ram B. Gupta received the B.E. degree in chemical engineering from the Indian Institute of Technology Roorkee, Roorkee, India, in 1987, the M.S. degree in chemical engineering from the University of Calgary, Calgary, AB, Canada, in 1989, and the Ph.D. degree in chemical engineering from The University of Texas at Austin, Austin, TX, USA, in 1993.

He is currently a Professor and an Associate Dean with the Faculty of Research Development, College of Engineering, Virginia Commonwealth University (VCU), Richmond, VA, USA. Prior to joining VCU, during 2011–2014, he was the Director of the Energy for Sustainability Program with the U.S. National Science Foundation. During 1995–2011, he was a Professor of Chemical Engineering with Auburn University. During 1993–1995, he did his postdoctoral work with the University of California, Berkeley, and under Management Development Program with Harvard University in 2018.

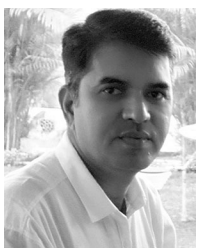

Babasaheb R. Sankapal received the Ph.D. degree from Shivaji University, Kolhapur, India, in 2001.

He is currently a Professor with the Department of Physics and an Associate Dean (Exam) with the Visvesvaraya National Institute of Technology, Nagpur, India, the Institute of National Importance. He was a Head and BoS Chairman (Physics) and is currently a Senate member. He was a Scientist with Helmholtz Centre (Hahn-Meitner Institute), Berlin, Germany; JSPS-PDF with Gifu University, Japan; and a Research Associate with the University of Wisconsin, Milwaukee, USA. He has authored or coauthored 133 publications (SCOPUS h-Index -33) and guided 13 Ph.D. students. His research interest includes synthesis of nanomaterials of inorganic semiconducting materials by using simple and low-cost chemical routes toward device grade solar cells, gas sensors, and supercapacitors developments.

Dr. Sankapal is a Fellow of MASc.